Biocompatible hydroxy double salts as delivery matrices for non-steroidal anti-inflammatory and anti-epileptic drugs

Abdessamad Y.A. Kaassis,[a,b] Wafa T. Al-Jamal,[b] Margarita Strimaite,[a] Maja Severic,[b] and Gareth R. Williams*[a]

a UCL School of Pharmacy, University College London, 29-39 Brunswick Square, London, WC1N 1AX, United Kingdom.
E-mail: g.williams@ucl.ac.uk

b School of Pharmacy, Queens's University Belfast, 97 Lisburn Rd, Belfast BT9 7BL, United Kingdom

Abstract

We recently reported the synthesis of two novel biocompatible hydroxy double salts (HDS), $[Mg_2Zn_3(OH)_8]Cl_2{\cdot}3.4H_2O$ (MgZn-Cl) and $[Fe_{2.4}Zn_{2.6}(OH)_8]Cl_2{\cdot}2H_2O$ (FeZn-Cl) (J. Mater. Chem. B 2016, 4, 5789) and showed them to be suitable for the loading and sustained release of naproxen. Here we build on these findings and report the intercalation, storage stability, biocompatibility and drug release properties of MgZn-Cl and FeZn-Cl loaded with diclofenac, ibuprofen, and valproate. All three active pharmaceutical ingredients could be successfully intercalated into both HDS by ion exchange. An increase in interlayer space from ca. 8 Å to 18.5 – 27 Å was observed after intercalation, consistent with the replacement of the initial chloride ion with the larger drug anions. Confirmation of successful intercalation was provided by IR spectroscopy, elemental microanalysis, and thermogravimetric analysis. ^{1}H NMR revealed that the structural integrity of the drug ions is not affected by intercalation. Drug release studies were performed in conditions representative of the gastrointestinal tract, and showed that the solubility of the drug ions controls the fate of the HDS in an acidic environment. The valproate intercalates dissolved completely within two hours at pH 1.0, whereas the other drug-loaded HDS freed some of their drug payload in the acidic media and the rest at pH 6.8. The HDS are further found to be biocompatible in an *in vitro* cell viability test, and to remain stable upon storage for 5 years.

Keywords: Hydroxy double salts • intercalation • sustained release • drug delivery • biocompatibility

1. Introduction

There has been huge progress in drug discovery science over recent years, which has led to many novel molecules with the ability to modernise the treatment and/or prevention of disease (Kaul et al., 1998; Jones et al., 2015). Delivering these drugs *in vivo* is usually confronted by barriers (e.g. low solubility, stability at a certain pH) (van de Waterbeemd and Testa, 2008; Savjani et al., 2012; Viswanathan et al., 2017). When an active pharmaceutical ingredient (API) is loaded into a carrier, its efficacy can be considerably enhanced (Hillery et al., 2001). For this reason, much research has been performed into designing degradable materials, intelligent delivery systems, and innovative delivery approaches (Langer, 1998). Nevertheless, the real challenge is to deliver both existing and new drugs in a way that benefits patients, healthcare workers and the healthcare system. Many of the carriers employed to modulate drug release are pH sensitive (Balamurali et al., 2011; Yoshida et al., 2013), allowing release to occur only under certain pH conditions. An ideal carrier should deliver its payload depending on the environmental composition, rather than relying on pH only.

Modern controlled release systems are usually polymer based (Nykänen et al., 1999; Zhang et al., 2014); much less attention has been paid to inorganic delivery systems (e.g. layered materials), even though they have a number of promising features. In layered materials, the atoms exhibit strong bonding connecting them in two dimensions, and much weaker bonding in the third dimension (Trifiro and Vaccari, 1996). This endows them with a wide ranging host/guest chemistry. There are many types of inorganic layered materials, such as layered double hydroxides (LDH) and hydroxy double salts (HDS). These are anionic clay materials, with structures derived from brucite and simonkolleite respectively. LDH have been widely explored as ion exchange materials. They have a hydrotalcite-like structure composed of positively charged metal hydroxide sheets and charge balancing anions in the interlayer space, with the general formula $[M^{z+}_{1-x}M^{3+}_{x}(OH)_2]^{q+}(X^{n-})_{q/n}\cdot yH_2O$. Generally, M^{z+} is a divalent metal ion (e.g.

Ni^{2+}), M^{3+} is a trivalent metal ion (e.g. Al^{3+}) and X is an anion (e.g. Cl^-) (Meyer and Sauvage, 2006). LDH have versatile applications in chemistry (Shao et al., 2014; Zhao et al., 2014; Dou et al., 2015; Kaassis et al., 2015; Tian et al., 2015), and also hold potential as drug delivery systems (Gao et al., 2018; Mei et al., 2018; Peng et al., 2018; Weng et al., 2018; Choi et al., 2019). In addition, LDHs possess inherent antacid properties (Xiao et al., 2011) . A clinical trial showed that hydrotalcite antacid acted more quickly and was more effective than other formulations (Holtmeier et al., 2007).

The HDS have similar same key structural features to the LDH, and their generic formula is $[(M^{2+}_{2-x}Me^{2+}_x)(OH)_{4-y}]X^{n-}_{y/n}\cdot zH_2O$. M^{2+} and Me^{2+} correspond to divalent metal ions (e.g. Zn^{2+}, Co^{2+}, Ni^{2+}, or Cu^{2+}) and X^{n-} is an exchangeable interlayer anion (e.g. Cl^- and NO_3^-) (Sathisha et al., 2012; Williams et al., 2012). One of the common HDS is the zinc basic salt (ZBS), $[Zn_5(OH)_8](NO_3)_2\cdot 2H_2O$ (Nowacki and Silverman, 1961; Allmann, 1968; Hawthorne and Sokolova, 2002). The ZBS is made of three Zn^{2+} ions occupying octahedral sites in hydroxide layers, with two additional Zn^{2+} cations situated above and below the layer in tetrahedral sites. HDS tend to be stable and inert, and have been investigated in the medical field as biomolecule reservoirs (Oh et al., 2009), antimicrobial/antifungal agents (Polson et al., 2009), and drug delivery systems (Ramli et al., 2013; Saifullah et al., 2013; Majoni and Hossenlopp, 2014; Nabipour et al., 2015). The HDS have received much less consideration than the LDH as drug delivery agents in particular, with only a handful of papers reported (Yang et al., 2007; Bull et al., 2011; Barahuie et al., 2014; Rojas et al., 2015). However, the data reported to date suggest that HDS loaded with APIs release their loading in a more sustained manner than LDH do (Arulraj et al., 2007; Selma et al., 2012).

While HDS can represent promising drug delivery systems, they are usually composed of toxic ions such as Cu^{2+} or Ni^{2+}. There is a risk that the HDS break down or metal ions leach from them during their gastrointestinal transit, which might lead to absorption of free metals (Powell et al., 1999). Thus, their approval by medicines agencies (e.g. the Food and Drug Administration (FDA) or European Medicines Agency (EMA)) around the globe will be challenging. This is because there are a number of serious concerns regarding the absorption and accumulation of inorganic materials in the body with repeated applications, and their potential systemic toxicity (Arruebo, 2012). Any putative inorganic drug delivery system must hence be composed of metals that are part of the natural composition of the human body. In case the component metals do become absorbed or accumulated, it is vital that they do not have any potential systemic toxicity.

New HDS containing biocompatible metals are thus sought after. Until 2016, there was only one reported attempt to synthesise a biocompatible HDS. In 1971, Stahlin and Oswald tried to synthesise an Mn/Zn HDS, but the reaction was not successful (Stählin and Oswald, 1971). Zinc is a vital trace element in humans, and the oral LD_{50} for $ZnCl_2$, $FeCl_2$ and $MgCl_2$ are around 350, 895 and 2800 mg/kg in rats, respectively. Thus, ZBS systems based on these metals should be less toxic than other HDS (Fosmire, 1990; Leitzmann and Giovannucci, 2004; Plum et al., 2010). In order to ameliorate this issue, we recently synthesised new HDSs based on Mg/Zn and Fe/Zn (Kaassis et al., 2016a). We further demonstrated that they could be used as delayed and extended release mechanisms for the non-steroidal anti-inflammatory drug (NSAID) naproxen.

The NSAIDs (e.g. ibuprofen, diclofenac and naproxen) are commonly used in the treatment of temporary (e.g. headache, muscle inflammation) or permanent pains (e.g. rheumatoid arthritis) (Kean and Buchanan, 2005; Affaitati et al., 2017). However; they can cause a range of side effects in the gastrointestinal system. New formulations are required to overcome the safety and

tolerability concerns associated with commercial NSAIDs (McCarberg and Gibofsky, 2012). Generally, antacids are co-prescribed with NSAIDs to prevent gastropathy (Becker et al., 2004). It was demonstrated that antacids such as magnesium hydroxide also reduce the lag time of ibuprofen and increase its diffusion rate, resulting in a rapid analgesic effect (Neuvonen, 1991). Since HDSs have similar compositions to $Mg(OH)_2$, they should also have antacid properties and be able to prevent gastropathy upon NSAID administration, as well as providing controlled release of an intercalated API.

Sodium valproate is indicated in the treatment of epilepsy (Pinder et al., 1977). Usually, prolonged valproate therapy causes gastritis in children and oral antacids are recommended to prevent degeneration (Marks et al., 1988). In addition, it was observed that such extended valproate application might lead to depletion of essential elements (e.g.: Zn and Mg) (Shah et al., 2001; Armutcu et al., 2004). These elements need to be monitored during the treatment period and metal supplement are recommended. Use of an HDS carrier for valproate could overcome both these issues, preventing gastric disorders through its buffering capability and releasing depleted essential elements as it dissolves to do so.

In this work, we looked to extend our work on biocompatible HDS systems to deliver commonly used drugs in a tuneable manner and reduce some of their side-effects. The sodium salts of ibuprofen (SI), diclofenac (Dic) and valproic acid (Val) were loaded into biocompatible Mg/Zn and Fe/Zn HDS through an ion- exchange route. The resulting products were characterised by X-ray diffraction, IR spectroscopy, NMR and elemental analysis. Drug release from the materials obtained was explored under conditions that mimic the human gastrointestinal tract. The biocompatibility of the two HDS and HDS/API intercalates was also investigated.

2. Experimental

2.1. Materials

Materials were obtained as follows: zinc oxide (ZnO) and magnesium chloride ($MgCl_2 \cdot 6H_2O$) (Fisher Scientific, Waltham, MA, USA); iron chloride ($FeCl_2 \cdot 4H_2O$), potassium iodide (KI), ibuprofen sodium (SI), naproxen sodium (Nap), and valproate sodium (Val) (Sigma; Gillingham, UK); diclofenac sodium (Dic) (Cambridge Bioscience, Cambridge, UK); RPMI 1640 media, FBS, penicillin-streptomycin, and L-glutamine (Gibco, Thermo Fisher, Waltham, MA, USA) All chemicals were used without further purification. Commercial tablets used as controls were Nurofen and Nurofen Express 200 mg (Reckitt Benckiser, Slough, UK), and Naprosyn (Roche, Basel, Switzerland).

2.2. HDS synthesis

Synthesis was performed following the methods reported in our previous study (Kaassis et al., 2016a). Following a range of optimisation studies, we prepared HDSs with M:Zn ratios as close to 1:1 as we could obtain. $[Mg_2Zn_3(OH)_8]Cl_2 \cdot yH_2O$ (MgZn-Cl) was synthesised by reaction of ZnO (20.0g) with $MgCl_2 \cdot 6H_2O$ (70.0 g) in 100 mL deionised water. The mixture was stirred for 3 days at room temperature, and the product recovered by vacuum filtration. The resultant white powder was rinsed with deionised water, and then allowed to dry under vacuum at 40 °C.

$[Fe_{2.4}Zn_{2.6}(OH)_8]Cl_2 \cdot yH_2O$ (FeZn-Cl) was prepared by reacting ZnO (5.0 g) with $FeCl_2 \cdot 4H_2O$ (11.8 g) in the presence of KI (3.0 g) in 100 mL deionised water. Air was excluded from the vial. The mixture was stirred for 3 days at room temperature, and the product recovered by vacuum filtration. The FeZn-Cl system tended to oxidise easily when in contact with air, and to minimise this water was rapidly drained from the preparation using a large filter funnel before the solid was washed with deionised water. The product was then dried in a vacuum oven in the presence of silica gel at 40 °C and 0 % humidity. The solid products were all inspected visually and showed no signs of the presence of solid I_2.

2.3. Intercalation

Intercalation of the organic anions was achieved by combining 0.4 mmol of the HDS with a 4-fold excess of the guest anions. 10 mL of deionised water was added to the solid materials, and the mixture stirred at 60 ºC for 4 days in a sealed glass vial. KI (0.2 mmol) was added to the mixture of FeZn-Cl and the organic guest anions to reduce HDS oxidation, and the vial flushed with N_2 before reaction. The solid products were filtered under vacuum, washed with deionised water, and dried. The intercalates of the FeZn-Cl HDS were treated with extra care as described above.

2.4. Characterisation

2.4.1. Materials characterisation

Scanning electron microscopy (SEM) was performed on a SUPRA 55 instrument (Zeiss, Oberkochen, Germany) with an accelerating voltage of 20 kV. The instrument was fitted with an energy dispersive X-ray (EDX) spectroscopy attachment for elemental analysis. Further SEM-EDX analysis was undertaken with a JSM-6701F microscope (JEOL, Tokyo, Japan) equipped with a INCAx-Act EDX detector (Oxford Instruments, Oxford, UK). The images obtained were analysed using the ImageJ software (National Institutes of Health, Bethesda, MD,USA) (ChemAxon, 2013). Additional SEM images were recorded on a Quanta 200 FEG ESEM microscope (FEI, Hillsborough, OR, USA), or a S-4800 microscope (Hitachi, Tokyo, Japan).

Powder X-ray diffraction (XRD) patterns were obtained using a MiniFlex 600 diffractometer (Rigaku, Tokyo, Japan), using Cu Kα radiation at 40 kV and 15 mA. IR spectra were collected on a Spectrum 100 instrument (PerkinElmer, Waltham, MA, USA). Data were recorded from 4000 to 650 cm^{-1} at a resolution of 2 cm^{-1}.

Nuclear magnetic resonance (NMR) experiments were carried out on a AV-400 spectrometer (Bruker, Billerica, MA, USA) operating at a ^{1}H frequency of 400.13 MHz. Samples were dissolved in D_2O for NMR analysis. C, H, and N contents were determined using the quantitative combustion technique on a CE1108 elemental analyser (Carlo Erba, Wigan, UK).

Thermogravimetric analysis was carried out on a Discovery TGA instrument (TA Instruments, New Castle, DE, USA). The sample (ca. 5-10 mg) was mounted in an aluminium pan and heated at a rate of 10 °C min^{-1} between 30 °C and 400 °C under a flow of nitrogen (10 mL min^{-1}).

2.4.2. Guest recovery

To ensure that the guest ions could be recovered intact from the intercalation compounds, the latter (50 mg) were reacted with Na_2CO_3 (100 mg) in 5 mL of D_2O overnight at 80 ºC. The samples were filtered, and ^{1}H NMR spectra collected on the filtrates. Samples of the pure drug were also dissolved in D_2O and analysed by NMR for comparison purposes.

2.4.3. Drug release

Drug release (dissolution) tests were carried out under experimental conditions mimicking as closely as possible the gastrointestinal tract and following pharmacopeia requirements (US Pharmacopeia USP 38NF33, 2015). The USP-II test (a paddle method) was used, with a PTWS instrument (PharmaTest, Hainburg, Germany) fitted with an inline spectrometer (CE 2500, Cecil, Cambridge, UK) being employed to perform these experiments. Samples were placed in 750 mL of 0.1 M HCl in a vessel held at 37 ± 0.5 °C, and stirred at 50 rpm. After 2 hours of operation, the pH of the medium was adjusted to 6.8 ± 0.05 by adding 250 mL of 0.20 M tribasic sodium phosphate. Experiments were carried out for 22 h at this pH. Dissolution tests were carried out in darkness, in triplicate with the new formulations prepared and 5 times with the commercial tablets.

2.4.4. Stability studies

Stability studies were carried out by storing the HDS and HDS-drug powders under standard environmental conditions in the laboratory (temperature and humidity varied with the seasons). The HDS and HDS-drugs intercalates were kept in glass vials and the stability was assessed after 3, 6, 12 and 60 months using FTIR, XRD and NMR.

2.4.5. Cytotoxicity

A preliminary proof of concept study was performed using a human prostate cancer (C4-2B) cell line was purchased from MD Anderson Cancer Center (Texas, USA). The cells were maintained in Advanced RPMI-1640 (1×) medium supplemented with 10% heat inactivated FBS, 1% penicillin/streptomycin and 2mM L-glutamine. The C4-2B cells (1×10^4) were seeded overnight in poly-d-lysine (100 µg mL^{-1}) coated 96-well culture plates (Sardstedt) in complete media. Next, the cells were incubated with 200 µL of the test compounds (MgZn-Cl, FeZn-Cl, MgZn-SI and FeZn-SI) at a final concentration of 5 µg/ml. The cytotoxicity was determined using the resazurin assay, as previously described (Pereira et al., 2019). Briefly, cells were incubated with 0.01 mg/mL resazurin solution for 4 h. After incubation, fluorescence (λ_{ex} = 544 nm, λ_{em} = 590 nm) was read using an automated FLUOstar Omega (BMG Labtech, UK) plate reader. The results were expressed as the percentage of cell viability (mean ± SEM) and normalised to vehicle-treated cells.

3. Results and discussion

3.1. Electron microscopy and elemental analysis

Scanning electron microscopy (SEM) images demonstrated that the MgZn-Cl starting material exhibited a symmetrical hexagonal particle shape and the FeZn-Cl an asymmetrical silhouette (Figures S1 and 2, Supplementary Information). The morphology observed here agrees well with the literature (Ziba et al., 2010; Delorme et al., 2011). Element mapping showed that both Mg/Fe and Zn are homogenously distributed throughout the HDS. The FeZn-Cl HDS additionally shows a side phase of iron and oxygen, which is often observed in Zn/Fe LDH systems.(Han et al., 2021)

SEM was also performed on selected intercalates, and images are given in Figure 1 and Figure S3. The FeZn-Val and MgZn-Val particles remained hexagonal after intercalation. In contrast, the intercalation of Dic into the MgZn-Cl led to the particle shape changing from hexagonal to rod shaped and the MgZn-SI and FeZn-SI particles had a sand-rose shape. Changes in the shape and size of particles suggest that the ion exchange reactions were not topotactic.

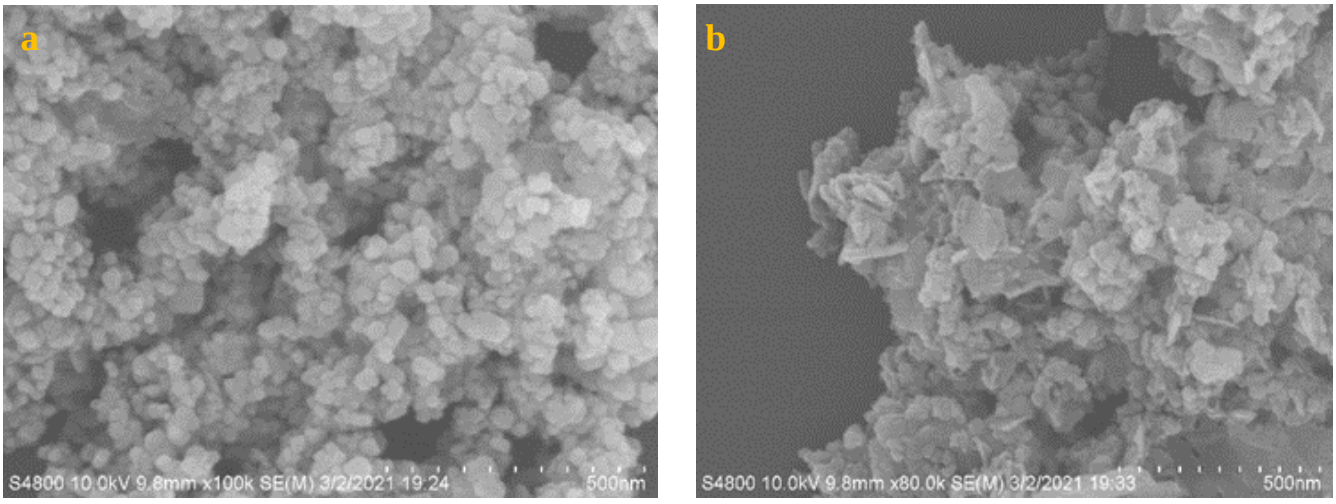

Figure 1: SEM images of **(a)** MgZn-SI and **(b)** FeZn-SI.

3.2. X-ray diffraction

The X-ray diffraction (XRD) data in Figure 2 showed that the preparation of the biocompatible HDS was successful, and in accordance with the previous report (Kaassis et al., 2016a). Their interlayer spaces are given in Table 1. FeZn-Cl had a dark green colour, which implies that the Fe^{2+} was d not oxidised to Fe^{3+} and remained in the divalent oxidation state.

XRD patterns of the drug intercalates of MgZn-Cl are also given in Figure 2. The reaction products showed no basal reflections characteristic of the starting material, and a shift of the *00l* basal reflections to lower angles; this corresponds to an increase in interlayer distance, which is indicative of the intercalation of a larger anion (Dic, SI and Val) into the interlayer galleries of the HDS by anion exchange for Cl. The interlayer space increased from 8.1 Å with MgZn-Cl to 18.8 Å, 22.8 Å, and 27.0 Å for the Val, Dic, and SI intercalates; respectively. These are in good agreement with the results reported in the literature on other types of HDS drug intercalates: d-values of 19.4 Å for Val, 22.3 Å for Dic, and 27.0 Å for SI have been noted previously (Taj et al., 2013; Kaassis et al., 2016b). All the diffraction patterns illustrated reflection broadening, indicative of stacking defects, except that of MgZn-Dic. Full data are included in Table 1.

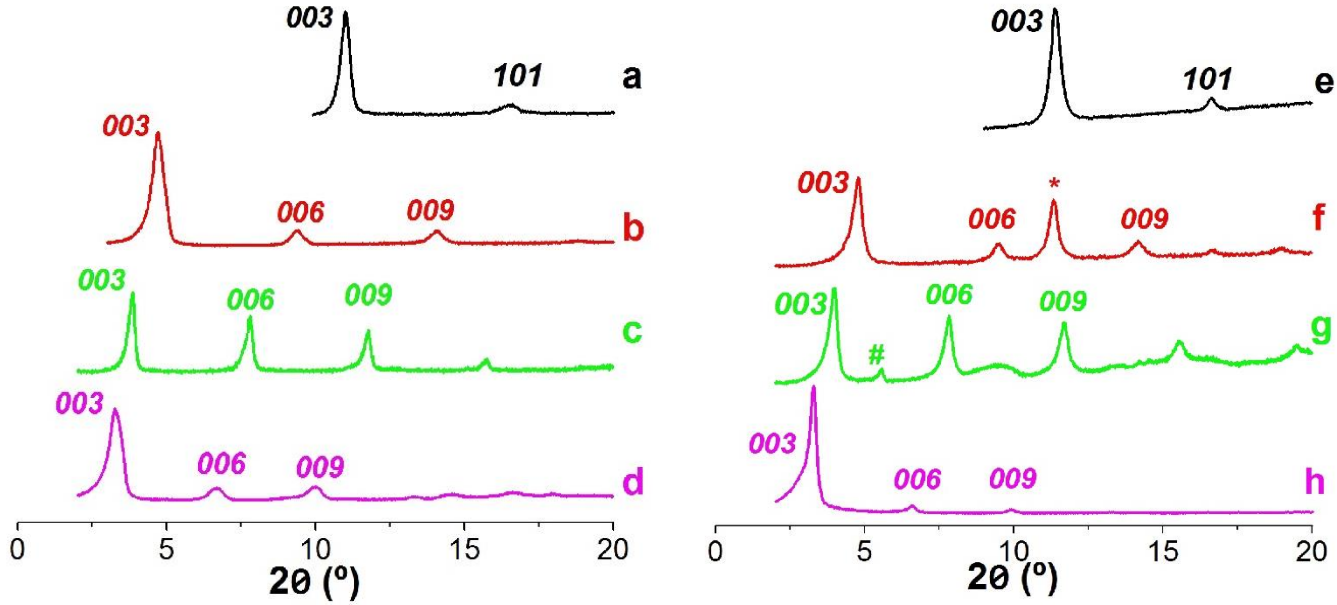

Figure 2: XRD patterns of **(a)** MgZn-Cl; **(b)** MgZn-Val; **(c)** MgZn-Dic; **(d)** MgZn-Sl; **(e)** FeZn-Cl; **(f)** FeZn-Val; **(g)** FeZn-Dic; and, **(h)** FeZn-Sl. * denotes residual starting material; # denotes a minority intercalate phase with reduced d-spacing.

Table 1: The interlayer spaces and chemical formulae of the various MgZn-drug and FeZn-drug composites prepared.

ID	d_{003} (Å)	Formula [a,b]	Elemental analysis (%) Obsd (calcd)[a]	Drug loading mass (%)
MgZn-Cl	7.9	$Mg_{2.1}Zn_{2.9}(OH)_8(Cl)_2 \cdot H_2O$	-	-
MgZn-Val	18.8	$Mg_{2.66}Zn_{2.34}(OH)_8(C_8H_{15}O_2)_{1.04}(CO_3)_{0.48} \cdot 4.0H_2O$	C 17.43 (17.51) H 4.02 (5.28)	24.68
MgZn-Dic	22.8	$Mg_{1.33}Zn_{3.67}(OH)_8(C_{14}H_{10}Cl_2NO_2)_2(C_{14}H_{11}Cl_2NO_2)_{0.32} \cdot 2.2H_2O$	C 34.46 (34.43) H 2.77 (3.20) N 1.44 (2.87)	60.46
MgZn-Sl	27.0	$Mg_{0.71}Zn_{4.29}(OH)_8(C_{13}H_{17}O_2)_{1.84}(CO_3)_{0.06} \cdot 1.9H_2O$	C 33.61 (33.68) H 4.52 (5.09)	44.02
FeZn-Cl	7.8	$Fe_{2.4}Zn_{2.6}(OH)_8Cl_2 \cdot H_2O$	-	-
FeZn-Val[c]	18.6	$Fe_{1.59}Zn_{3.41}(OH)_8(C_8H_{15}O_2)_{0.61}(Cl)_{1.39} \cdot 3.4H_2O$	C 9.12 (9.08) H 2.18 (3.74)	13.53
FeZn-Dic[c]	22.4/ 15.9	$Fe_{2.87}Zn_{2.13}(OH)_8(C_{14}H_{10}Cl_2NO_2)_{1.62}(CO_3)_{0.19} \cdot 4.4H_2O$	C 27.32 (27.35) H 2.72 (3.31) N 2.34 (2.26)	47.60
FeZn-Sl	26.9	$Fe_{1.46}Zn_{3.54}(OH)_8(C_{13}H_{17}O_2)_{0.91}(CO_3)_{0.40}(Cl)_{0.29} \cdot 3.9H_2O$	C 19.83 (19.84) H 3.16 (4.26)	25.23

[a] C and H contents were determined by quantitative combustion. The metal ratios were quantified from EDX data.
[b] H_2O content was obtained from thermogravimetric analysis.
[c] It should be noted that these systems are biphasic. The formula depicted is an overall empirical formula for the solid material isolated.

The intercalation of the guests into the Fe-containing HDS was challenging, as the drug-loaded system tended to oxidise easily when in contact with air. This could be overcome by draining water from the preparation quickly, then drying the drug intercalates in a vacuum oven. Similar to the MgZn-Cl HDS, the basal reflections of the host could no longer be seen after intercalation (Figure 2), except for the intercalation of Val where the presence of some residual starting material could be seen (reflections of the host are marked with *****). The interlayer space increased from 7.8 Å with FeZn-Cl to 18.6 Å, 22.4/15.9 Å, and 26.9 Å for the Val, Dic, and SI intercalates, respectively. These were similar to the results reported above using the MgZn-Cl system. For FeZn-Dic there appeared to be two different intercalate phases; it was thought that one contained a bilayer of the guest (22.4 Å) and the other a monolayer (15.9 Å). A small reflection believed to correspond to the latter was marked # in Figure 2. A similar finding was observed during the intercalation of the Dic into a Ni/Zn HDS, where the molecular dynamics simulation showed the presence of a monolayer in the lower d-value system (Kaassis et al., 2016b).

The chemical formulae of the intercalates were assessed by energy-dispersive X-ray spectroscopy (EDX) and elemental microanalysis. Water content was determined by thermogravimetric analysis. SEM-EDX images are given in Figures S4 and S5, and a summary of the data in Table 1. On the basis of CHN microanalysis, in a number of cases it appeared that there was less drug intercalated than needed to charge balance. For some systems (FeZn-SI and FeZn-Val), Cl could be observed by EDX, indicating incomplete replacement of the initial interlayer anion. In other systems, no Cl was visible and thus we hypothesise that carbonate ions were present, which is consistent with the literature (Conterosito et al., 2015; Hibino, 2018) and high affinity of the HDS systems for CO_3^{2-}. Further, some leaching of metal ions was noted after intercalation, such that the ratios of metals in the final product was not the same as in the starting materials. This is consistent with the SEM observations and confirms a non-topotactic ion exchange process.

3.3. IR spectroscopy

The IR spectra of MgZn-Cl and FeZn-Cl are depicted in Figures 3a and S6a. Both HDS showed two bands with shoulders around 3500 and 3460 cm^{-1}, which could be ascribed to stretches of the OH groups of the layers and water molecules (both in the interlayer and adsorbed on the particle surfaces), respectively. There was also a band around 1603 cm^{-1} which could be assigned to the δ-bend of water molecules. Vibration bands at 1030 and 900 cm^{-1} arose from the bending of M-OH groups and those in the region of 530 and 460 cm^{-1} from M–O and O–M–O vibrations (M = Mg and Fe). The spectrum of pure SI (Figures 3) contained distinct OH stretches around 3000–3500 cm^{-1} due to the presence of water in the material (SI is very hygroscopic and typically exists as the dihydrate form). Bands assigned to alkane C–H stretches were located between 3000–2850 cm^{-1}, and carboxylate asymmetric and symmetric stretches at 1546 and 1406 cm^{-1} (respectively). These had the same band shape, which was indicative of the ionic form (Figure S7a) (Mehrotra and Bohra, 1983).

The infrared spectra of the SI intercalation products (MgZn-SI and FeZn-SI) are given in Figures 3b and S6b. They presented a very broad adsorption band centred at around 3400 cm^{-1} that could be assigned to the OH stretching vibration of hydroxyl groups. Bands assigned to alkane C–H stretches were visible between 3000–2850 cm^{-1}, with no obvious changes in the band positions or intensities observed. The SI carboxylate vibrations did show some changes however, and doublets were observed in the asymmetric and symmetric stretches located at 1567/1535 and 1393/1382 cm^{-1}; respectively (Figure S7). This suggested that there was a new bonding mode between the carboxylate ligand and the HDS layers. There was an increase in intensity for the asymmetric stretching band and a reduction in the symmetric stretching vibration, demonstrating that the symmetry of the SI carboxylate group in the HDS was lower than that of the carboxylate group in the ionic form. This was a sign of only one oxygen atom being coordinated with the metal cation, resulting in a monodentate interaction between the SI

carboxylate ligand and a metal cation of the HDS layer (Mehrotra and Bohra, 1983; Palacios et al., 2004).

The IR spectra for the other intercalation compounds all displayed analogous features: all the characteristic bands of the drug ions were present after intercalation and demonstrated that the intact guests were successfully intercalated in both HDS. In the raw drug salts, the asymmetric and symmetric carboxylic stretches had similar band shapes and roughly equal intensities, but after intercalation the asymmetric stretch had a greater intensity, as noted for MgZn-SI. The stretch positions before and after intercalation for the MgZn formulations are summarised in Table S1. The values noted were similar to literature data for monodentate zinc/diclofenac, and zinc/valproate complexes (Darawsheh et al., 2014; Abu Ali and Jabali, 2016). This suggests that there was a monodentate interaction between the guest carboxylate ligand and a tetrahedral metal ion on the HDS layers.

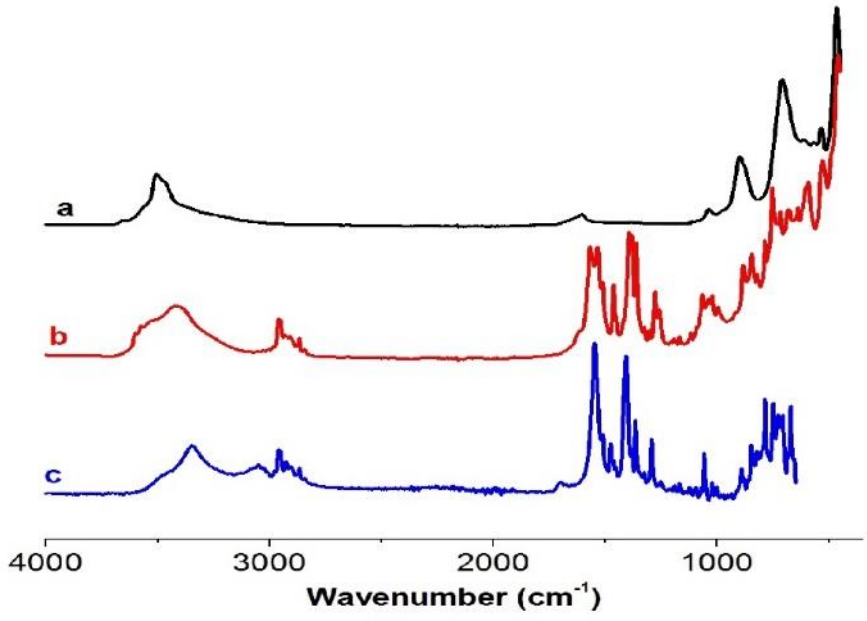

Figure 3: IR spectra of (**a**) MgZn-Cl, (**b**) MgZn-SI, and (**c**) SI raw material.

3.4. Thermogravimetric analysis

Thermogravimetric analysis (TGA) was performed on various HDS materials, which showed between two and three stages as is usually observed with LDH and HDS materials. For MgZn-Cl (Figure S8a), mass loss went through three phases. The first two losses of 5 % and 7 %, which ended by 120 ºC and 200 ºC, correspond to adsorbed water molecules on the external surface and interlayer water molecules. The final loss of 13 % began around 300 ºC and is related to layer dehydration or dehydroxylation. The dehydroxylation of MgAl-Cl LDH was reported to begin at a similar temperature (Constantino and Pinnavaia, 1995). For FeZn-Cl (Figure S8b), mass loss went through two stages, the initial mass loss of 6.5 % was complete by 160 ºC and corresponds to loss of two water molecules. The dehydroxylation event of FeZn-Cl occurred between 150-250 ºC, at lower temperature than MgZn-Cl, which suggests that MgZn-Cl is more thermally stable than FeZn-Cl.

TGA traces of the intercalates (Figure S8) revealed mass loss in three stages, except for MgZn-Dic. This is usual for organic guests intercalated into HDS materials (Bull et al., 2011; Liu et al., 2015). The initial mass loss (*ca.* 3.5 – 12 %) and the second loss are expected to correspond to the loss of surface adsorbed and interlayer water molecules. The third stage of mass loss corresponded to the HDS layer dehydroxylation and initiation of interlayer guest anion degradation. These decomposition and dehydroxylation events are overlapping and cannot be resolved. However, it should be noted that there was no obvious decomposition of the SI was observed in MgZn-SI. Most of the HDS materials showed these three stages occurring between 60 and 300ºC. The exception is MgZn-Dic, where the first mass loss of *ca.* 4 % was complete by 90 ºC and corresponded to the loss of surface adsorbed water molecules.

3.5. Guest orientation

The layer thickness of the HDS is around 8.5 Å (from end to end of the tetrahedral units), while the thickness of the flat octahedral sections is around 5 Å. The lengths of the guest ions were

calculated (using the Marvin software (ChemAxon, 2013)) to be 4.48 Å (Val); 10.02 Å (Dic); and 10.38 Å (SI). Comparing the lengths of the guests with the interlayer space minus the HDS layer thickness suggested that the interlayer space was between 1.5 and 2 times the length of the intercalated ions. This suggested that the guests adopted intertwined bilayer or bilayer arrangements, with the carboxylic acid groups pointing towards the positively charged layers. For SI and Val, the interlayer space was around twice the size of the molecules, suggesting a perpendicular bilayer arrangement of ions. For Dic, the interlayer space was greater than the size of one molecule and less than the length of two, indicating an intertwined bilayer arrangement. Based on these considerations, a schematic of the guest orientations in the MgZn system is provided in Figure S9. The FeZn system had very similar interlayer spaces, and thus analogous arrangements were envisaged. For the FeZn-Dic minority phase seen in the XRD pattern at 15.9 Å (Figure 2g), the Dic ions were expected to be arranged in a perpendicular monolayer.

3.6. Guest recovery

The MgZn-Dic, MgZn-SI, MgZn-Val, FeZn-Dic, FeZn-SI and FeZn-Val intercalates were each reacted with Na_2CO_3 in D_2O, and NMR spectra recorded of the filtrate from these reactions. The spectra after deintercalation were observed to be identical to those of the Dic, SI and Val starting materials, confirming that the structural integrity of these drug molecules was retained. For instance, the ^1H NMR spectrum of de-intercalated SI contained resonances at: 0.9 ppm corresponding to the methyl protons of the isobutyl group; at 1.39 ppm ascribed to the α-methyl protons; at 2.47 ppm originating from the methylene adjacent to the phenyl group; at 1.83 ppm arising from the methine proton of the isobutyl moiety; at 3.62 ppm due to the α-methine proton; and at 7.24 ppm, resulting from the four benzene protons. Those results were similar to the pristine SI (Figure S10). Analogous results were seen for the other guest ions (data not shown).

3.7. Drug release

The drug release of the four APIs loaded into HDS was performed in simulated physiological conditions representative of the human gastrointestinal tract, and compared to some commercial formulations. For comparison purposes, we also presented here data from our previous report on naproxen (Nap) intercalates of these HDS (Kaassis et al., 2016a). The drug release plots are depicted in Figure 4. Table S2 gives a summary of the release profiles for all the APIs from intercalated HDS and commercial formulations.

The *in vitro* release profiles of SI from the MgZn-SI powder and selected commercial tablets (Nurofen and Nurofen Express) are presented in Figure 4a. Both commercial tablets disintegrated quickly but the SI embedded did not completely dissolve. The SI concentration remained low throughout the acid immersion period due to its low solubility at low pH. On the other hand, some of the MgZn-SI material was dissolved in acidic media, freeing SI in a gradual manner into the solution and resulting in slightly higher release than the commercial systems. Once the pH was adjusted to 6.8, the remaining SI from the commercial tablets dissolved within 5 min. However; SI release from MgZn-SI occurred slowly over 2 hours. It was believed that there were two release mechanisms which took place: firstly, leaching (at low pH), followed by ion exchange (at pH ≥ 6.8, and reliant on the presence of phosphate anions). Many release studies were carried out using LDH-SI powders in phosphate buffer (pH ≥ 7) (Ambrogi et al., 2001; Gunawan and Xu, 2008, 2009; Huang et al., 2011; Lu et al., 2013), but few studies were carried out in acidic media (pH < 3) since it is known that LDH dissolve at low pH (Choy et al., 2000). Barkhordari and co-workers reported that more than 80 % of an Mg/Al LDH-SI formulation was dissolved within 2 h at pH 1.2 (Barkhordari et al., 2014). Hence, the MgZn-SI HDS system appeared to be somewhat more stable than Mg/Al LDH-SI in acidic media.

393 The release of Dic from the MgZn-Dic and FeZn-Dic systems and selected commercial capsules
394 (Diclomac® SR 75mg) is shown in Figure 4b and summarised in Table S2. The MgZn-Dic, FeZn-
395 Dic and commercial formulation behaved similarly in acid media with low release rates and less
396 than 3% of the drug cargo freed into solution. When the pH was increased to 6.8, the release
397 rate increased in all three cases. The MgZn-Dic, FeZn-Dic and Diclomac® formulations released
398 90% of their loading after 5, 7 and 10 h, respectively.

399 The *in vitro* dissolution profiles of Val from MgZn-Val and FeZn-Val are given in Figure 4c. After
400 1 h at pH 1, the FeZn-Val released only 50 % of its loading, versus 100 % from MgZn-Val (Table
401 S2). This was very different to Val release from analogous LDH systems at pH 1.2: as soon as
402 Zn/Al LDH-Val was in added to the acidic media, it was observed to dissolve giving a very rapid
403 burst release (Yazdani et al., 2019).

404 The *in vitro* dissolution of Nap from MgZn-Nap, FeZn-Nap and commercial tablets (Naprosyn®)
405 was reported in our previous study (Kaassis et al., 2016a). Naprosyn tablets disintegrated in a
406 short period of time, but Nap did not completely dissolve in the acidic solution. On the other
407 hand, Nap was gradually released from FeZn-Nap and MgZn-Nap. Once the pH was adjusted
408 from 1.0 to 6.8 the remaining Nap from Naprosyn dissolved within 5 min. While MgZn-Nap
409 behaved similarly to Naprosyn, the FeZn-Nap system gave a more sustained release profile
410 (Figure 4d and Table S2). The concentration of Nap released in the acidic solution was higher
411 for both HDS compared to the Naprosyn tablets; this implies that the solubility of Nap in acidic
412 media was enhanced in the presence of HDS. The improvement could be related to the release
413 of the drug in the ionic (rather than the salt) form from the dissolved FeZn-Nap and MgZn-Nap.
414 FeZn-Nap appeared to be a little more stable than MgZn-Nap in acidic media. Both leaching at
415 low pH and then ion exchange (pH ≥ 6.8) were believed to have contributed to release.

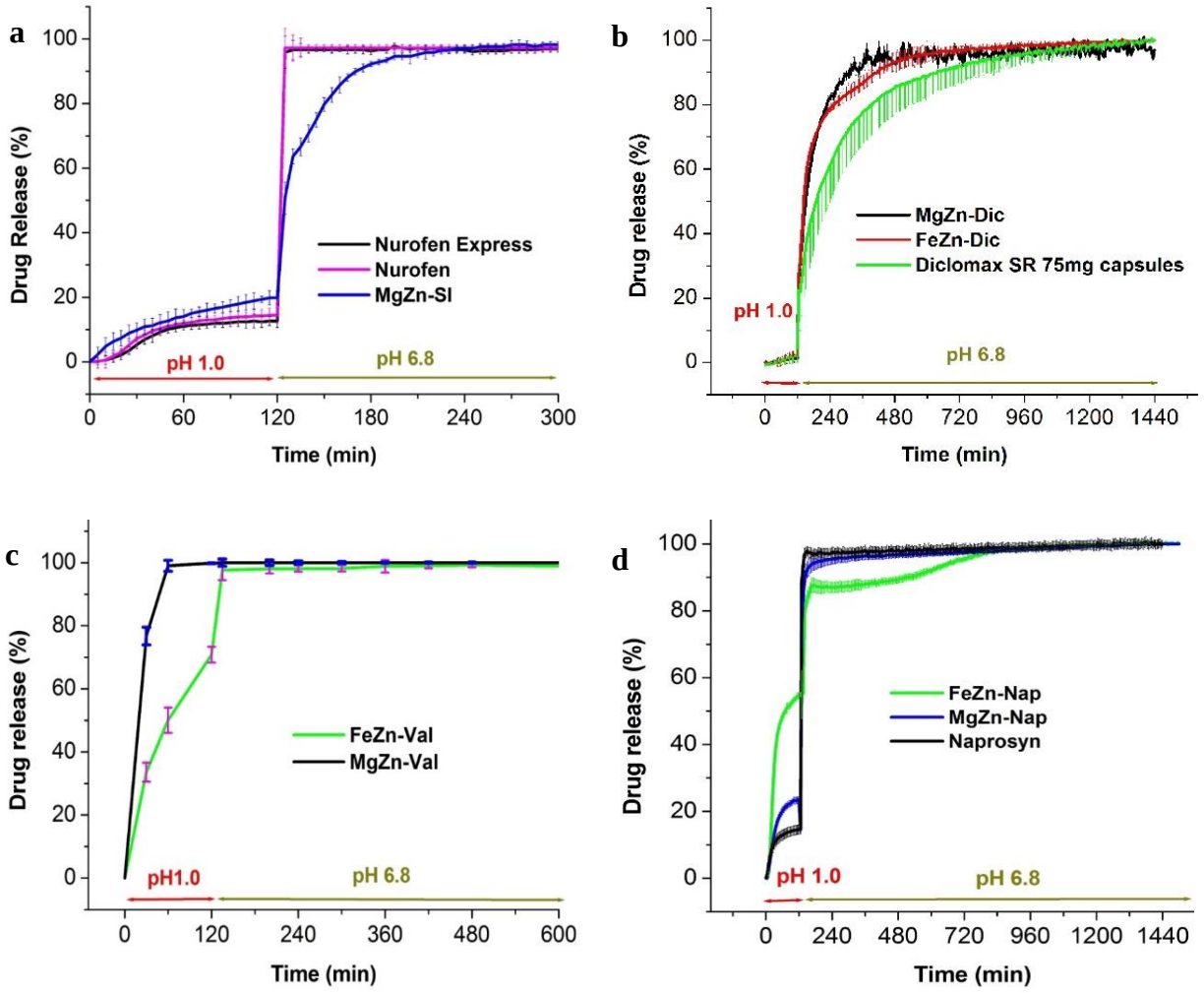

Figure 4: Drug release at pH 1 and pH 6.8. **(a)** SI release from MgZn-SI and two commercial formulations (Nurofen® and Nurofen Express®); **(b)** Dic release from FeZn-Dic, MgZn-Dic and commercial formulation (Diclomax® SR); **(c)** Val release from MgZn-Val and FeZn-Val; and **(d)** Nap release from FeZn-Nap, MgZn-Nap and a commercial formulation (Naprosyn®).

It was observed that HDS-Val can dissolve easily in acidic media, whereas HDS-SI and HDS-Nap partially dissolved and HDS-Dic remained almost intact. The solubility order of the four APIs in acidic media is as follows: Val > Nap > SI > Dic (Table S3).

This largely mirrored the extent of drug release seen after 120 min. When the HDS were in the acidic media, the outer layers (L0) dissolved and exposed guests that were bound to the first layer (L1) beneath it. Then, guests get freed from that layer which resulted in exposure of the second layer (L2) and so on. This mechanism kept going until the guest's solubility reached its

saturation level, and after that guests attached to the exposed layer (Ln) did not get liberated and acted as a shell protecting the remaining HDS layers from the acidic media (Figure 5). Thus, the solubility of the guest seemed to control the fate of the HDS in acidic media.

At pH 6.8, the release rate of Dic remained the slowest, followed by SI and Nap, with Val releasing most quickly. The release rate seemed to be governed by the API solubility, which lied in the same order in neutral conditions as in acidic media (Table S3).

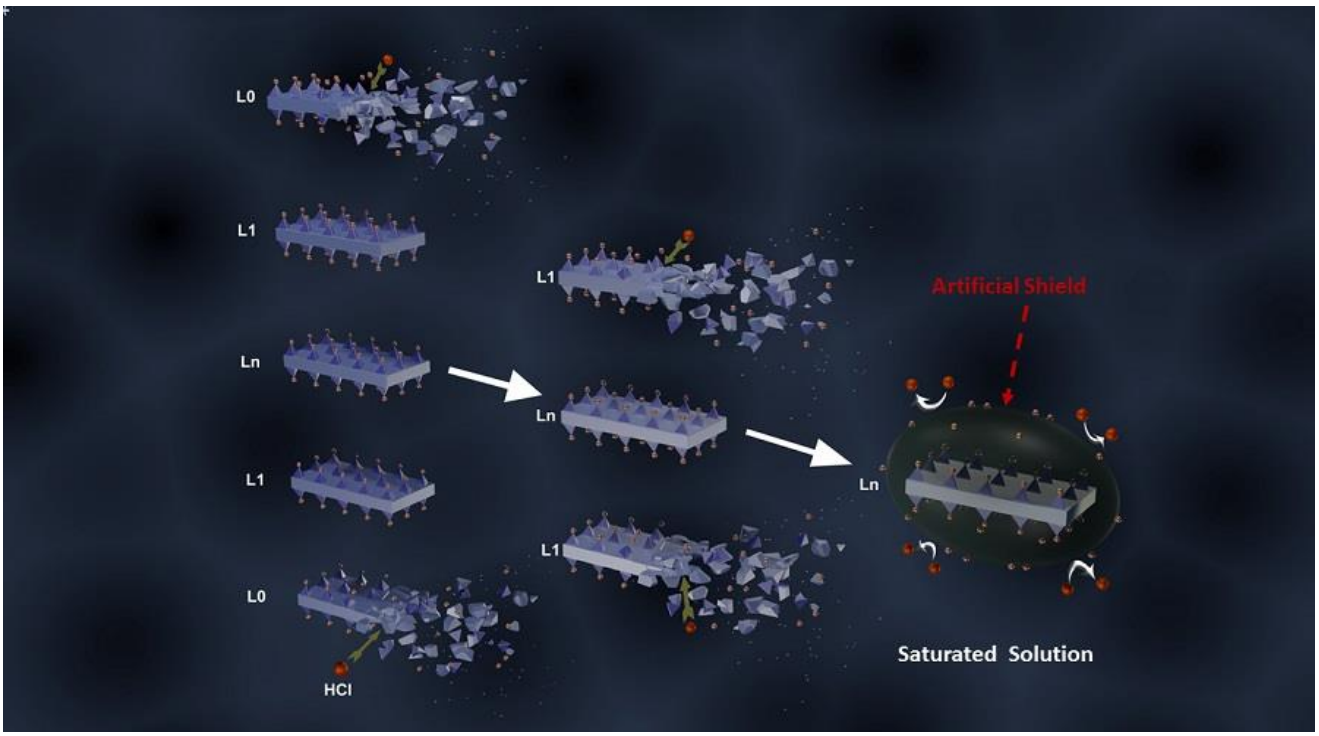

Figure 5: A schematic illustrating the HDS behaviour in an acidic media.

3.8. Stability

Many drugs were intercalated into LDH and HDS, but to the best of our knowledge no stability studies were reported. Both starting HDS and two HDS-drug candidates were selected for a stability test, one with an intertwined bilayer arrangement (MgZn-Dic) and one with a perpendicular bilayer arrangement (MgZn-SI). The stability study was carried out by storing powders under normal environmental conditions (temperature and humidity varying with the

438 seasons) in our lab in London, UK. The powders were kept in glass vials and stability tests were
439 performed at 0 days and after 1, 3, 12 and 60 months of storage using FTIR, XRD, and NMR.
440 The XRD and FTIR data of MgZn-Cl and FeZn-Cl showed no obvious changes during the five
441 years storage period (Figure S11-14). In addition, FeZn-Cl remained green and no visual
442 oxidation was observed.

443 The XRD patterns of MgZn-Dic revealed a decline in the d-value upon storage and the
444 appearance of a second, lower d-value phase. Two distinct phases were very clearly present
445 after five years, with d-values at 20.2 Å and 15.3 Å (Figure S15). This was first noted after 3
446 months storage, and reached a plateau after 12 months. The intercalation of Dic into an HDS
447 were observed to proceed via intermediates with similar d-value when studied *in situ* (Kaassis
448 et al., 2016b). The decrease in d-value could be due to the rearrangement of guests in the
449 interlayer spaces to reach a lower energy state. The IR spectra of MgZn-Dic after five years was
450 similar to the fresh sample but with a slight increase in the intensity of the OH stretches at around
451 3400 cm^{-1}. This was caused by an increase in the water content of the system (Figure S16).
452 Overall, however, it was clear that the two samples remained stable after five years' storage
453 and showed no sign of degradation.

454 For MgZn-SI, the XRD data showed that there was a decrease in the d-value from 27.0 Å to
455 24.7 Å after storage (Figure 6). Conterosito and co-workers reported that the *in-situ* intercalation
456 of SI into an LDH went through intermediates with similar d-value (Conterosito et al., 2013).
457 From the IR data no differences were observed after storage for any period of time except slight
458 changes in the carboxylate band intensity, and a slight rise in the intensity of the OH bands at
459 3425 cm^{-1} and 1614 cm^{-1} suggesting there was more water present after storage (Figure S17).
460 The ^{1}H NMR spectrum for the SI recovered from the intercalate after 5 years contained
461 resonances at 0.9, 1.39, 2.47, 1.83, 3.62 and 7.24 ppm, confirming the structural integrity of SI

462 and that no degradation had occurred within five years (Figure S18), which was similar to the
463 pristine SI (Figure S10). Most SI commercial tablets have two to three year shelf lives (e.g:
464 Nurofen®), and a stability study on commercial SI tablets disclosed between seven and ten
465 degradation products in three year-old samples (Farmer et al., 2002). The data obtained here
466 thus suggested that the HDS materials were more stable than commercial formulations.
467

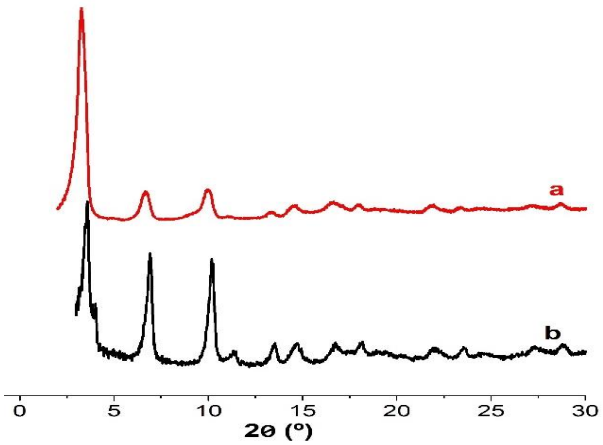

Figure 6: XRD patterns of MgZn-SI after storage for (**a**) one day and (**b**) five years

468

469 **3.9. Cytotoxicity**

470 To evaluate the biocompatibility of the new HDSs (MgZn-Cl, FeZn-Cl) and those loaded with SI
471 (MgZn-SI and FeZn-SI), constructs were incubated with a human prostate cancer (C4-2B) cell
472 line for 48 h. No reduction in cell viability was observed in all treatment groups (Figure 7),
473 indicating the high biocompatibility of our HDSs.

474 Generally, LDH cytotoxicity is considered moderate and varies according to the chemical
475 compositions (Choi and Choy, 2011). For instance, some *in vitro* experiments reported a drop
476 in cell viability (5-15%) following incubation with Zn/Al or Mg/Al LDHs (Choy et al., 2004; Choi
477 et al., 2008; Kura et al., 2014). The preliminary data presented here therefore indicate that our
478 new HDS materials might have greater cytocompatibility than LDHs. However, further studies

479 are required to evaluate in detail the safety of our HDSs in comparison to LDHs, using a range
480 of primary and cancer cell lines.

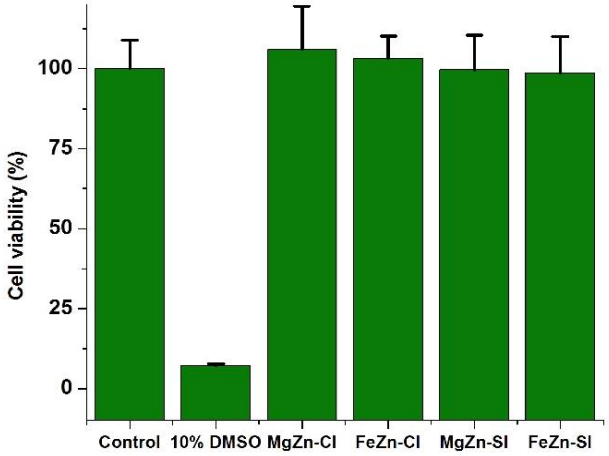

Figure 7: Cell viability of C4-2B cells incubated for 48 h with various HDS (n=4).

481 ## 4. Conclusions

482 This work builds on a recent study in which we reported the synthesis of two novel biocompatible
483 hydroxyl double salts (HDS), $Mg_2Zn_3(OH)_8(Cl)_2 \cdot 3.4H_2O$ (MgZn-Cl) and $Fe_{2.4}Zn_{2.6}(OH)_8Cl_2 \cdot 2H_2O$
484 (FeZn-Cl) (J. Mater. Chem. B 2016, 4, 5789). Diclofenac, ibuprofen, and valproate were loaded
485 into the two HDS by ion exchange. All three active pharmaceutical ingredients could be
486 successfully intercalated into both HDS, with an increase in interlayer space (from ca. 8 Å to
487 18.5 – 27 Å) consistent with the replacement of the initial chloride ion with the larger drug anions
488 observed by X-ray diffraction. The distances between the HDS layers indicate that the diclofenac
489 ions are arranged in an intertwined bilayer in the interlayer space, while ibuprofen and valproate
490 form bilayers. IR spectra of the intercalates show characteristic peaks of the drug anions,
491 confirming successful intercalation and revealing intermolecular interactions between the drug
492 and HDS layers. Proton NMR spectra of the drug ions were the same before and after
493 intercalation, indicating that the structural integrity of the drug ions is not affected by
494 intercalation. Drug release studies performed in conditions representative of the gastrointestinal
495 tract proved that the solubility of the drug ions controls the fate of the HDS in an acidic

environment. The valproate intercalates dissolved completely within two hours at pH 1.0, whereas the other drug-loaded HDS freed some of their drug loading in the acidic media and the rest at pH 6.8. The HDS are found to be biocompatible, and to remain stable upon storage for 5 years. These findings are promising for potential clinical adoption of HDS-based drug delivery systems.

Acknowledgements

The authors would like to thank Stephen Boyer of London Metropolitan University for elemental microanalysis measurements, and David McCarthy and Prof Abdul Basit (both UCL School of Pharmacy) for SEM images and access to the automated dissolution system respectively. This work was begun while AYAK was a visiting student at the Beijing University of Chemical Technology, as part of the Sino–UK Higher Education Research Partnership for PhD Studies funded by the British Council China and China Scholarship Council. We thus also thank these bodies.

Appendix A. Supplementary data

Supporting information for this article can be found online at

References

Abu Ali, H., Jabali, B., 2016. Synthesis, characterization and biological activity of novel complexes of zinc(II) diclofenac with nitrogen based ligands. Polyhedron 107, 97–106. https://doi.org/10.1016/j.poly.2016.01.010

Affaitati, G., Martelletti, P., Lopopolo, M., Tana, C., Massimini, F., Cipollone, F., Lapenna, D., Giamberardino, M.A., Costantini, R., 2017. Use of Nonsteroidal Anti-Inflammatory Drugs for Symptomatic Treatment of Episodic Headache. Pain Pract. 17, 392–401. https://doi.org/10.1111/papr.12461

Allmann, R., 1968. Verfeinerung der Struktur des Zinkhydroxidchlorids II, Zn 5 (OH) 8 Cl 2 · 1H 2 O. Zeitschrift für Krist. 126, 417–426. https://doi.org/10.1524/zkri.1968.126.5-6.417

Ambrogi, V., Fardella, G., Grandolini, G., Perioli, L., 2001. Intercalation compounds of hydrotalcite-like anionic clays with antiinflammatory agents - I. Intercalation and in vitro release of ibuprofen. Int. J. Pharm. 220, 23–32. https://doi.org/10.1016/S0378-5173(01)00629-9

Armutcu, F., Ozerol, E., Gurel, A., Kanter, M., Vural, H., Yakinci, C., Akyol, O., 2004. Effect of long-term therapy with sodium valproate on nail and serum trace element status in epileptic children. Biol. Trace Elem. Res. 102, 1–10. https://doi.org/10.1385/BTER:102:1-3:001

Arruebo, M., 2012. Drug delivery from structured porous inorganic materials. Wiley Interdiscip. Rev. Nanomedicine Nanobiotechnology 4, 16–30. https://doi.org/10.1002/wnan.132

Arulraj, J., Rajamathi, J.T., Prabhu, K.R., Rajamathi, M., 2007. Anionic clays as hosts for

anchored synthesis: Interlayer bromination of maleate and fumarate ions in nickel–zinc layered hydroxy double salt. Solid State Sci. 9, 812–816. https://doi.org/10.1016/j.solidstatesciences.2007.06.007
Balamurali, V., Pramodkuma, T.M., Srujana, N., Venkatesh, M.P., Gupta, N.V., Krishna, K.L., Gangadhara, H.V., 2011. pH Sensitive Drug Delivery Systems: A Review. Am. J. Drug Discov. Dev. 1, 24–48. https://doi.org/10.3923/ajdd.2011.24.48
Barahuie, F., Hussein, M.Z., Abd Gani, S., Fakurazi, S., Zainal, Z., 2014. Anticancer nanodelivery system with controlled release property based on protocatechuate-zinc layered hydroxide nanohybrid. Int. J. Nanomedicine 9, 3137–3149. https://doi.org/10.2147/IJN.S59541
Barkhordari, S., Yadollahi, M., Namazi, H., 2014. PH sensitive nanocomposite hydrogel beads based on carboxymethyl cellulose/layered double hydroxide as drug delivery systems. J. Polym. Res. 21, 1–9. https://doi.org/10.1007/s10965-014-0454-z
Becker, J.C., Domschke, W., Pohle, T., 2004. Current approaches to prevent NSAID-induced gastropathy--COX selectivity and beyond. Br. J. Clin. Pharmacol. 58, 587–600. https://doi.org/10.1111/j.1365-2125.2004.02198.x
Bull, R.M.R., Markland, C., Williams, G.R., O'Hare, D., 2011. Hydroxy double salts as versatile storage and delivery matrices. J. Mater. Chem. 21, 1822. https://doi.org/10.1039/c0jm03020a
ChemAxon, 2013. Marvin 6.0.1.
Choi, G., Piao, H., Eom, S., Choy, J.-H., 2019. Vectorized Clay Nanoparticles in Therapy and Diagnosis. Clays Clay Miner. 67, 25–43. https://doi.org/10.1007/s42860-019-0009-9
Choi, S.-J., Choy, J.-H., 2011. Effect of physico-chemical parameters on the toxicity of inorganic nanoparticles. J. Mater. Chem. 21, 5547. https://doi.org/10.1039/c1jm10167f
Choi, S.J., Oh, J.M., Choy, J.H., 2008. Safety aspect of inorganic layered nanoparticles: Size-dependency in vitro and in vivo. J. Nanosci. Nanotechnol. 8, 5297–5301. https://doi.org/10.1166/jnn.2008.1143
Choy, J.-H., Jung, J.-S., Oh, J.-M., Park, M., Jeong, J., Kang, Y.-K., Han, O.-J., 2004. Layered double hydroxide as an efficient drug reservoir for folate derivatives. Biomaterials 25, 3059–3064. https://doi.org/10.1016/j.biomaterials.2003.09.083
Choy, J.-H., Park, J., Kwak, S.-Y., Jeong, Y.-J., 2000. Inorganic Layered Double Hydroxides as Nonviral Vectors. Angew. Chem. Int. Ed. 39, 4041–4045. https://doi.org/10.1002/1521-3773(20001117)39:22<4041::AID-ANIE4041>3.0.CO;2-C
Constantino, V.R.L., Pinnavaia, T.J., 1995. Basic Properties of Mg2+1-xAl3+x Layered Double Hydroxides Intercalated by Carbonate, Hydroxide, Chloride, and Sulfate Anions. Inorg. Chem. 34, 883–892. https://doi.org/10.1021/ic00108a020
Conterosito, E., Palin, L., Antonioli, D., Viterbo, D., Mugnaioli, E., Kolb, U., Perioli, L., Milanesio, M., Gianotti, V., 2015. Structural Characterisation of Complex Layered Double Hydroxides and TGA-GC-MS Study on Thermal Response and Carbonate Contamination in Nitrate- and Organic-Exchanged Hydrotalcites. Chem. - A Eur. J. 21, 14975–14986. https://doi.org/10.1002/chem.201500450
Conterosito, E., Van Beek, W., Palin, L., Croce, G., Perioli, L., Viterbo, D., Gatti, G., Milanesio, M., 2013. Development of a Fast and Clean Intercalation Method for Organic Molecules into Layered Double Hydroxides. Cryst. Growth Des. 13, 1162–1169. https://doi.org/10.1021/cg301505e
Darawsheh, M., Abu Ali, H., Abuhijleh, A.L., Rappocciolo, E., Akkawi, M., Jaber, S., Maloul, S., Hussein, Y., 2014. New mixed ligand zinc(II) complexes based on the antiepileptic drug sodium valproate and bioactive nitrogen-donor ligands. Synthesis, structure and biological properties. Eur. J. Med. Chem. 82, 152–163. https://doi.org/10.1016/j.ejmech.2014.01.067
Delorme, F., Seron, a., Giovannelli, F., Beny, C., Jean-Prost, V., Martineau, D., 2011. Synthesis and anion exchange properties of a Zn/Co double hydroxide salt. Solid State Ionics 187, 93–97. https://doi.org/10.1016/j.ssi.2011.02.006
Dou, Y., Zhang, S., Pan, T., Xu, S., Zhou, A., Pu, M., Yan, H., Han, J., Wei, M., Evans, D.G., Duan, X., 2015. TiO 2 @Layered Double Hydroxide Core-Shell Nanospheres with Largely Enhanced Photocatalytic Activity Toward O 2 Generation. Adv. Funct. Mater. 25, 2243–2249. https://doi.org/10.1002/adfm.201404496
Farmer, S., Anderson, P., Burns, P., Velagaleti, R., 2002. Forced degradation of ibuprofen in bulk drug and tablets: Determination of specificity, selectivity, and the stability-indicating

590 nature of the USP ibuprofen assay method. Pharm. Technol. North Am. 26, 28–42.
591 Fosmire, G.J., 1990. Zinc toxicity. Am. J. Clin. Nutr. 51, 225–7.
592 Gao, R., Mei, X., Yan, D., Liang, R., Wei, M., 2018. Nano-photosensitizer based on layered
593 double hydroxide and isophthalic acid for singlet oxygenation and photodynamic therapy.
594 Nat. Commun. 9, 2798. https://doi.org/10.1038/s41467-018-05223-3
595 Gunawan, P., Xu, R., 2009. Direct assembly of anisotropic layered double hydroxide (LDH)
596 nanocrystals on spherical template for fabrication of drug-LDH hollow nanospheres.
597 Chem. Mater. 21, 781–783. https://doi.org/10.1021/cm803203x
598 Gunawan, P., Xu, R., 2008. Direct control of drug release behavior from layered double
599 hydroxides through particle interactions. J. Pharm. Sci. 97, 4367–4378.
600 https://doi.org/10.1002/jps.21321
601 Han, J., Xing, H., Song, Q., Yan, H., Kang, J., Guo, Y., Liu, Z., 2021. A ZnO@CuO core–shell
602 heterojunction photoanode modified with ZnFe-LDH for efficient and stable
603 photoelectrochemical performance. Dalt. Trans. 50, 4593–4603.
604 https://doi.org/10.1039/D1DT00336D
605 Hawthorne, F.C., Sokolova, E., 2002. SIMONKOLLEITE, Zn5 (OH)8 Cl2 (H2O), A
606 DECORATED INTERRUPTED-SHEET STRUCTURE OF THE FORM [M 2]4. Can.
607 Mineral. 40, 939–946. https://doi.org/10.2113/gscanmin.40.3.939
608 Hibino, T., 2018. Anion Selectivity of Layered Double Hydroxides: Effects of Crystallinity and
609 Charge Density. Eur. J. Inorg. Chem. 2018, 722–730.
610 https://doi.org/10.1002/ejic.201701067
611 Hillery, A., Lloyd, A., Swarbrick, J., 2001. Drug delivery and targeting for pharmacists and
612 pharmaceutical scientists, Nature. Taylor & Francis, London.
613 Holtmeier, W., Holtmann, G., Caspary, W.F., Weingärtner, U., 2007. On-demand treatment of
614 acute heartburn with the antacid hydrotalcite compared with famotidine and placebo:
615 randomized double-blind cross-over study. J. Clin. Gastroenterol. 41, 564–70.
616 https://doi.org/10.1097/MCG.0b013e31802e7efb
617 Huang, W., Zhang, H., Pan, D., 2011. Study on the release behavior and mechanism by
618 monitoring the morphology changes of the large-sized drug-LDH nanohybrids. AIChE J.
619 57, 1936–1946. https://doi.org/10.1002/aic.12379
620 Jones, C.L., Yeung, B.K.S., Manjunatha, U., Shi, P.-Y., Bodenreider, C., Diagana, T.T., 2015.
621 Drug discovery for the developing world: progress at the Novartis Institute for Tropical
622 Diseases. Nat. Rev. Drug Discov. 14, 442–444. https://doi.org/10.1038/nrd4001-c1
623 Kaassis, A.Y.A., Wei, M., Williams, G.R., 2016a. New biocompatible hydroxy double salts and
624 their drug delivery properties. J. Mater. Chem. B 4, 5789–5793.
625 https://doi.org/10.1039/c6tb01108j
626 Kaassis, A.Y.A., Xu, S., Evans, D.G., Williams, G.R., Wei, M., Duan, X., 2015. Combined In
627 Situ and In Silico Studies of Guest Intercalation into the Layered Double Hydroxide [LiAl 2
628 (OH) 6]X· y H 2 O. J. Phys. Chem. C 119, 18729–18740.
629 https://doi.org/10.1021/acs.jpcc.5b04203
630 Kaassis, A.Y.A., Xu, S.M., Guan, S., Evans, D.G., Wei, M., Williams, G.R., 2016b. Hydroxy
631 double salts loaded with bioactive ions: Synthesis, intercalation mechanisms, and
632 functional performance. J. Solid State Chem. 238, 129–138.
633 https://doi.org/10.1016/j.jssc.2016.03.019
634 Kaul, P.N., Edwards, G., Weston, A.H., Rohmer, M., Rockhold, R.W., Johnson, T.D., Colacino,
635 J.M., Staschke, K.A., 1998. Progress in Drug Research. Birkhäuser Basel, Basel.
636 https://doi.org/10.1007/978-3-0348-8833-2
637 Kean, W.F., Buchanan, W.W., 2005. The use of NSAIDs in rheumatic disorders 2005: a global
638 perspective. Inflammopharmacology 13, 343–70.
639 https://doi.org/10.1163/156856005774415565
640 Kura, A.U., Ain, N.M., Hussein, M.Z., Fakurazi, S., Hussein-Al-Ali, S.H., 2014. Toxicity and
641 metabolism of layered double hydroxide intercalated with levodopa in a Parkinson's
642 disease model. Int. J. Mol. Sci. 15, 5916–5927. https://doi.org/10.3390/ijms15045916
643 Langer, R., 1998. Drug delivery and targeting. Nature 392, 5–10.
644 Leitzmann, M.F., Giovannucci, E., 2004. RESPONSE: Re: Zinc Supplement Use and Risk of
645 Prostate Cancer. JNCI J. Natl. Cancer Inst. 96, 1108–1109.
646 https://doi.org/10.1093/jnci/djh207
647 Liu, J., Wang, J., Zhang, X., Fang, B., Hu, P., Zhao, X., 2015. Preparation and structural

characterization of zwitterionic surfactant intercalated into NiZn–layered Hydroxide Salts. J. Phys. Chem. Solids. https://doi.org/10.1016/j.jpcs.2015.05.017
Lu, X., Meng, L., Li, H., Du, N., Zhang, R., Hou, W., 2013. Facile fabrication of ibuprofen–LDH nanohybrids via a delamination/reassembling process. Mater. Res. Bull. 48, 1512–1517. https://doi.org/10.1016/j.materresbull.2012.12.057
Majoni, S., Hossenlopp, J.M., 2014. Controlled Release Kinetics in Hydroxy Double Salts: Effect of Host Anion Structure. Adv. Phys. Chem. 2014, 1–12. https://doi.org/10.1155/2014/710487
Marks, W.A., Morris, M.P., Bodensteiner, J.B., Grunow, J.E., Bobele, G.B., Hille, M.R., Tuggle, D., 1988. Gastritis with valproate therapy. Arch. Neurol. 45, 903–5. https://doi.org/10.1001/archneur.1988.00520320101022
McCarberg, B., Gibofsky, A., 2012. Need to Develop New Nonsteroidal Anti-Inflammatory Drug Formulations. Clin. Ther. 34, 1954–1963. https://doi.org/10.1016/j.clinthera.2012.08.005
Mehrotra, R.., Bohra, R., 1983. Metal carboxylates, 3rd ed. Academic Press, New york.
Mei, X., Ma, J., Bai, X., Zhang, X., Zhang, S., Liang, R., Wei, M., Evans, D.G., Duan, X., 2018. A bottom-up synthesis of rare-earth-hydrotalcite monolayer nanosheets toward multimode imaging and synergetic therapy. Chem. Sci. 9, 5630–5639. https://doi.org/10.1039/c8sc01288a
Meyer, P.D.T.J., Sauvage, H.W.R.J., 2006. Layered Double Hydroxides, Structure and Bonding. Springer-Verlag, Berlin/Heidelberg. https://doi.org/10.1007/b100426
Nabipour, H., Hosaini Sadr, M., Thomas, N., 2015. Synthesis, characterisation and sustained release properties of layered zinc hydroxide intercalated with amoxicillin trihydrate. J. Exp. Nanosci. 10, 1269–1284. https://doi.org/10.1080/17458080.2014.998301
Neuvonen, P.J., 1991. The effect of magnesium hydroxide on the oral absorption of ibuprofen, ketoprofen and diclofenac. Br. J. Clin. Pharmacol. 31, 263–266. https://doi.org/10.1111/j.1365-2125.1991.tb05527.x
Nowacki, W., Silverman, J.N., 1961. Die Kristallstruktur von Zinkhydroxychlorid II, Zn 5 (OH) 8 Cl 2 · 1H 2 O*. Zeitschrift für Krist. 115, 21–51. https://doi.org/10.1524/zkri.1961.115.1-2.21
Nykänen, P., Krogars, K., Säkkinen, M., Heinämäki, J., Jürjensson, H., Veski, P., Marvola, M., 1999. Organic acids as excipients in matrix granules for colon-specific drug delivery. Int. J. Pharm. 184, 251–261. https://doi.org/10.1016/S0378-5173(99)00114-3
Oh, J.-M., Biswick, T.T., Choy, J.-H., 2009. Layered nanomaterials for green materials. J. Mater. Chem. 19, 2553. https://doi.org/10.1039/b819094a
Palacios, E.G., Juárez-López, G., Monhemius, A.J., 2004. Infrared spectroscopy of metal carboxylates. Hydrometallurgy 72, 139–148. https://doi.org/10.1016/S0304-386X(03)00137-3
Peng, L., Mei, X., He, J., Xu, J., Zhang, W., Liang, R., Wei, M., Evans, D.G., Duan, X., 2018. Monolayer Nanosheets with an Extremely High Drug Loading toward Controlled Delivery and Cancer Theranostics. Adv. Mater. 30, 1707389. https://doi.org/10.1002/adma.201707389
Pereira, S.G.T., Hudoklin, S., Kreft, M.E., Kostevsek, N., Stuart, M.C.A., Al-Jamal, W.T., 2019. Intracellular Activation of a Prostate Specific Antigen-Cleavable Doxorubicin Prodrug: A Key Feature Toward Prodrug-Nanomedicine Design. Mol. Pharm. 16, 1573–1585. https://doi.org/10.1021/acs.molpharmaceut.8b01257
Pinder, R.M., Brogden, R.N., Speight, T.M., Avery, G.S., 1977. Sodium valproate: a review of its pharmacological properties and therapeutic efficacy in epilepsy. Drugs 13, 81–123. https://doi.org/10.2165/00003495-197713020-00001
Plum, L.M., Rink, L., Haase, H., 2010. The Essential Toxin: Impact of Zinc on Human Health. Int. J. Environ. Res. Public Health 7, 1342–1365. https://doi.org/10.3390/ijerph7041342
Polson, G.A., Roberts, K.P., Lou, K.K., Dinicola, K.N., 2009. Compositions and methods for nail fungus treatment. WO2009148794 A1.
Powell, J.J., Jugdaohsingh, R., Thompson, R.P., 1999. The regulation of mineral absorption in the gastrointestinal tract. Proc. Nutr. Soc. 58, 147–153. https://doi.org/10.1079/PNS19990020
Ramli, M., Hussein, M.Z., Yusoff, K., 2013. Preparation and characterization of an anti-inflammatory agent based on a zinc-layered hydroxide-salicylate nanohybrid and its effect

on viability of Vero-3 cells. Int. J. Nanomedicine 8, 297–306. https://doi.org/10.2147/IJN.S38858
Rojas, R., Linck, Y.G., Cuffini, S.L., Monti, G. a., Giacomelli, C.E., 2015. Structural and physicochemical aspects of drug release from layered double hydroxides and layered hydroxide salts. Appl. Clay Sci. 109–110, 119–126. https://doi.org/10.1016/j.clay.2015.02.030
Saifullah, B., Hussein, M.Z., Hussein-Al-Ali, S.H., Arulselvan, P., Fakurazi, S., 2013. Sustained release formulation of an anti-tuberculosis drug based on para-amino salicylic acid-zinc layered hydroxide nanocomposite. Chem. Cent. J. 7, 72. https://doi.org/10.1186/1752-153X-7-72
Sathisha, T.V., Kumara Swamy, B.E., Chandrashekar, B.N., Thomas, N., Eswarappa, B., 2012. Selective determination of dopamine in presence of ascorbic acid and uric acid at hydroxy double salt/surfactant film modified carbon paste electrode. J. Electroanal. Chem. 674, 57–64. https://doi.org/10.1016/j.jelechem.2012.03.020
Savjani, K.T., Gajjar, A.K., Savjani, J.K., 2012. Drug Solubility: Importance and Enhancement Techniques. ISRN Pharm. https://doi.org/10.5402/2012/195727
Selma, S.., Richardson-Chong, Patel, R., Williams, G.R., 2012. Intercalation and Controlled Release of Bioactive Ions Using a Hydroxy Double Salt. Ind. Eng. Chem. Res. 51, 2913–2921. https://doi.org/10.1021/ie202036y
Shah, Q., Jamil, A., Gupta, V., Kabiraj, M., Shah, A., 2001. Changes in serum electrolytes in childhood epilepsy: A hospital-based prospective. Greenwich J Sci Technol 2, 18–27.
Shao, M., Ning, F., Wei, M., Evans, D.G., Duan, X., 2014. Hierarchical Nanowire Arrays Based on ZnO Core−Layered Double Hydroxide Shell for Largely Enhanced Photoelectrochemical Water Splitting. Adv. Funct. Mater. 24, 580–586. https://doi.org/10.1002/adfm.201301889
Stählin, W., Oswald, H.R., 1971. The topotactic reaction of zinc hydroxide nitrate with aqueous metal chloride solutions. J. Solid State Chem. 3, 256–264. https://doi.org/10.1016/0022-4596(71)90038-7
Taj, S.F., Singer, R., Nazir, T., Williams, G.R., 2013. The first hydroxy double salt tablet formulation. RSC Adv. 3, 358. https://doi.org/10.1039/c2ra21339g
Tian, R., Zhang, S., Li, M., Zhou, Y., Lu, B., Yan, D., Wei, M., Evans, D.G., Duan, X., 2015. Localization of Au Nanoclusters on Layered Double Hydroxides Nanosheets: Confinement-Induced Emission Enhancement and Temperature-Responsive Luminescence. Adv. Funct. Mater. 25, 5006–5015. https://doi.org/10.1002/adfm.201501433
Trifiro, F., Vaccari, A., 1996. Comprehensive supramolecular chemistry. Compr. Supramol. Chem. 34, 34-5097-34–5097. https://doi.org/10.5860/CHOICE.34-5097
US Pharmacopeia USP 38NF33, 2015. The United States Pharmacopeial Convention, (711) Dissolution. Rockville,MD. 486–496.
van de Waterbeemd, H., Testa, B., 2008. Drug Bioavailability, Methods and Principles in Medicinal Chemistry. Wiley-VCH Verlag GmbH & Co. KGaA, Weinheim, Germany. https://doi.org/10.1002/9783527623860
Viswanathan, P., Muralidaran, Y., Ragavan, G., 2017. Challenges in oral drug delivery: a nano-based strategy to overcome, in: Nanostructures for Oral Medicine. Elsevier, pp. 173–201. https://doi.org/10.1016/B978-0-323-47720-8.00008-0
Weng, Y., Guan, S., Lu, H., Meng, X., Kaassis, A.Y., Ren, X., Qu, X., Sun, C., Xie, Z., Zhou, S., 2018. Confinement of carbon dots localizing to the ultrathin layered double hydroxides toward simultaneous triple-mode bioimaging and photothermal therapy. Talanta 184, 50–57. https://doi.org/10.1016/j.talanta.2018.02.093
Williams, G.R., Crowder, J., Burley, J.C., Fogg, A.M., 2012. The selective intercalation of organic carboxylates and sulfonates into hydroxy double salts. J. Mater. Chem. 22, 13600. https://doi.org/10.1039/c2jm32257a
Xiao, R., Wang, W., Pan, L., Zhu, R., Yu, Y., Li, H., Liu, H., Wang, S.-L., 2011. A sustained folic acid release system based on ternary magnesium/zinc/aluminum layered double hydroxides. J. Mater. Sci. 46, 2635–2643. https://doi.org/10.1007/s10853-010-5118-8
Yang, J., Han, Y., Park, M., Park, T., Hwang, S., Choy, J., 2007. New Inorganic-Based Drug Delivery System of Indole-3-Acetic Acid-Layered Metal Hydroxide Nanohybrids with Controlled Release Rate. Chem. Mater. 19, 2679–2685.

https://doi.org/10.1021/cm070259h
Yazdani, P., Mansouri, E., Eyvazi, S., Yousefi, V., Kahroba, H., Hejazi, M.S., Mesbahi, A., Tarhriz, V., Abolghasemi, M.M., 2019. Layered double hydroxide nanoparticles as an appealing nanoparticle in gene/plasmid and drug delivery system in C2C12 myoblast cells. Artif. Cells, Nanomedicine Biotechnol. 47, 436–442. https://doi.org/10.1080/21691401.2018.1559182
Yoshida, T., Lai, T.C., Kwon, G.S., Sako, K., 2013. pH- and ion-sensitive polymers for drug delivery. Expert Opin. Drug Deliv. 10, 1497–1513. https://doi.org/10.1517/17425247.2013.821978
Zhang, Z., Qi, X., Li, X., Xing, J., Zhu, X., Wu, Z., 2014. A novel pulsatile drug delivery system based on the physiochemical reaction between acrylic copolymer and organic acid: In vitro and in vivo evaluation. Int. J. Pharm. 462, 66–73. https://doi.org/10.1016/j.ijpharm.2013.12.026
Zhao, J., Chen, J., Xu, S., Shao, M., Zhang, Q., Wei, F., Ma, J., Wei, M., Evans, D.G., Duan, X., 2014. Hierarchical NiMn Layered Double Hydroxide/Carbon Nanotubes Architecture with Superb Energy Density for Flexible Supercapacitors. Adv. Funct. Mater. 24, 2938–2946. https://doi.org/10.1002/adfm.201303638
Ziba, A., Paculła, A., Serwicka, E.M., Drelinkiewicz, A., 2010. Transesterification of triglycerides with methanol over thermally treated Zn5(OH)8(NO3)2×2H 2O salt. Fuel 89, 1961–1972. https://doi.org/10.1016/j.fuel.2009.11.013